INSTITUTO POLITÉCNICO DE BRAGANÇA
Escola Superior de Tecnologia e Gestão

Evaluation of new carbon-coating methods for the development of magnetic nanoparticles targeted for biomedical applications

Nerea Seoane Magallanes

Thesis report submitted to

Escola Superior de Tecnologia e Gestão

Instituto Politécnico de Bragança

Master Degree in

Chemical Engineering

Supervisors:

Prof. Helder Teixeira Gomes

Dr. Jose Luis Díaz de Tuesta Triviño

Bragança

October 2021

ACKNOWLEDGEMENTS

Practical and scientific support were essential to develop this work, but emotional support was decisive during this time. Related to this last support, I extend my acknowledgements to all my family and friends who stayed with me this last year.

I would like to thank the researchers who were with me during the lab work for the availability, support and teaching given, in especially to Adriano dos Santos Silva and Fernanda Fontana Roman.

Thanks to Dr. Helder T. Gomes and Dr. Jose L. Diaz de Tuesta for guidance during all this project and the opportunity given to work with them in this research.

At last, I thank IPB and Centro de Investigaçao de Montanha for all the structure and material provided to carry out the research.

ABSTRACT

Nanoscience has recently experienced a strong development, Magnetic Nanoparticles (MNPs) are one of the most attractive nanomaterials. Focusing on the biomedical applications, this thesis has as main objective the development of new carbon coating methods in order to reach the maximum biocompatibility of MNPs upon synthesis.

During the research carried out, two different approaches were evaluated to coat a magnetic core composed of magnetite, using phloroglucinol and glyoxal, following the idea of making the process more sustainable and biocompatible. The difference between those approaches resides on the use of PF-127 as porogen agent during the coating step. However, some significant differences were found for the material synthesized without PF-127 as porogen agent, with the most important one being the lack of stabilization in water, a crucial characteristic of MNPs for biomedical applications. This mishap leaded to the continuation of the methodology development with just one material.

The material selected was evaluated as nanocarrier to load and deliver drugs using doxorubicin (DOX) and omeprazole (OME). The delivery was tested at different pH values in order to evaluate its influence, as human body has different pH in a normal tissue (pH 7.4) than in the intracellular tumor environment (pH 4.5) or in its surroundings (pH 6.0).

Keywords: nanomaterials; magnetic; biomedicine; coating; drug delivery.

RESUMO

A nanociência tem experimentado recentemente um forte desenvolvimento. As nanopartículas magnéticas (MNPs) têm sido um dos materiais mais atraentes. Com foco nas aplicações biomédicas, esta tese tem como objetivo principal desenvolver novos métodos de revestimento de carbono para alcançar a máxima biocompatibilidade durante a síntese de MNPs.

Durante a pesquisa serão avaliadas duas abordagens diferentes para revestir um núcleo magnético feito de magnetita, as duas utilizan floroglucinol e glioxal, seguindo a ideia de tornar o processo mais sustentável e biocompatível. A diferença entre essas abordagens será sobre o emprego da PF-127 como agente porógeno durante a etapa de revestimento. No entanto, algumas diferenças significativas foram encontradas que o material sintetizado sem a PF-127 como agente porógeno não estava arquivando uma das características mais importantes das MNPs para aplicações biomédicas, a estabilização na água. Este mishap conduziu a continuar a metodologia apenas com um material.

O material selecionado foi avaliado para carga e entrega de medicamentos com doxorrubicina e omeprazol. A entrega foi testada em diferentes valores de pH para avaliar sua influência, pois o corpo humano tem pH diferente em um tecido normal (pH 7,4) do que no ambiente tumoral intracelular (pH 4,5) ou em seu entorno (pH 6,0).

Palabras chave: nanomateriais; magnético; biomedicina; revestimento; entrega de medicamentos.

Summary

List of abbreviations

CS	Core/shell
DLC	Drug loading capacity
DLE	Drug loading efficiency
DOX	Doxorubicin
FESEM	Field emission scanning electron microscopy
MNPs	Magnetic nanoparticles
MRI	Magnetic resonance imaging
OMCs	Ordered mesoporous carbons
OME	Omeprazole
USP	Ultrasonic spray pyrolysis
YS	Yolk/shell

List of figures

List of tables

INTRODUCTION

1. Introduction

The wide interdisciplinary world of nanoscience has experienced a strong development in recent years. One interesting topic is the possibility of using nanoscale magnetic materials for biomedical applications, applying encapsulation of magnetic cores to produce biocompatible magnetic nanoparticles (MNPs). Coating the MNPs with a suitable material offers the possibility to attach them to antibodies, proteins, and medical drugs, among others. Therefore, studies on surface adsorption, and the possibility of functionalizing and/or conjugating the particle coating with bioactive components are also crucial issues. The election of the magnetic material, as well as detailed knowledge of its magnetic properties, play an important role in the use of MNPs in biomedicine, and in the effectiveness of the desired application [1].

Typically, carbon coating methods consider covering the magnetic cores with noxious substances, such as hydroxybenzene and formaldehyde resins for further carbonization at a controlled temperature and atmosphere. For this reason, the development of methods including more benign reagents are required.

1.1. Objective

The objective of this work is to evaluate new carbon-coating methods for the development of MNPs targeted for biomedical applications. It includes the exploration of more benign reagents than those typically used (hydroxybenzene and formaldehyde) and different synthesis conditions (pressure, temperature, among others) than those used in previous works for the carbon-coating of MNPs. The developed MNPs are further evaluated in drug loading and delivery using doxorubicin, a known drug used the treatment of cancer, and omeprazole.

STATE OF THE ART

2. State of the art

2.1. Magnetic Nanoparticles

MNPs are a group of particles (typically smaller than 100 nm) that can be controlled under the influence of an external magnetic field [2].

The factors that influence the magnetic properties of nanoparticles include their chemical composition, crystal lattice, particle shape, size and microstructure, morphology, and the way that MNPs interact with adjacent particles or with the surrounding matrix [3,4].

As the size of the particles decrease, interesting magnetic properties appear, which differ from those of conventional bulk materials, due to the nanoscale confinement and surface defects [3].

Exploring the properties of the large surface-to-volume ratio of the nanoparticles (for sizes lower than 100 nm) is of critical importance and has led to the discovery of novel physical, chemical, and mechanical properties, when compared to those of the corresponding bulk material as they have higher reactivities. The factors influencing the critical size of the single domain are the shape of the particles, the strength of the crystal anisotropy, the value of the magnetic saturation, and the wall energy domain [3,5].

2.2. Applications

MNPs are particularly promising in several biomedical applications, such as cellular therapy involving cell labeling and targeting as a tool for cell-biology research to separate and purify cell populations, tissue repair, targeted drug delivery, magnetic resonance imaging (MRI) and hyperthermia for cancer treatment, among others [4], as illustrated in Figure 1.

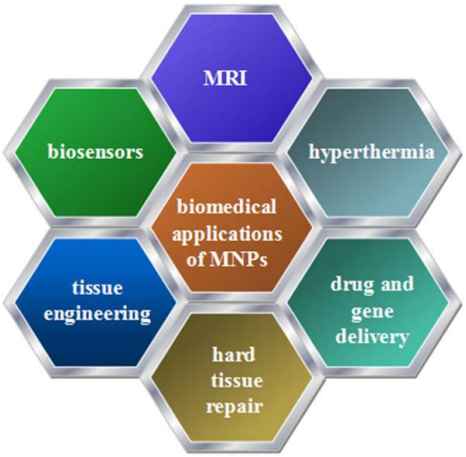

***Figure 1**: Examples of biomedical applications of MNPs* [5].

The biocompatibility and toxicity of the nanoparticles are important criteria to consider them for biomedical applications. The parameters determining these criteria are the nature of the magnetically responsive component and the final size of the composite particles including their core and coatings (shell). Ideally, the composites must also have a high magnetization so that their movement in the blood can be controlled with an external magnetic field until it is immobilized close to the targeted pathological tissue [6].

Two kinds of applications can be distinguished: in vivo applications and in vitro applications. The in vivo applications include targeted drug delivery, magnetic resonance imaging, magnetic hyperthermia, and thermoablation. On the other hand, the in vitro applications can include bioseparation and biosensors [6].

2.2.1. Cancer therapy

MNPs have been studied for the detection, diagnosis, and treatment of malignant tumors. Different sizes of MNPs exhibit different characteristics. Ferromagnetism with large size can be used to alternate magnetic hysteresis under heat and be used in cancer targeted therapy. MNPs with small sizes are suitable for hyperthermia [5].

Following surgery, radiotherapy, chemotherapy, and immunotherapy, hyperthermia treatment has become the fifth largest method in cancer therapy and it is applied in clinical practice. In magnetic hyperthermia a heat generating material is inserted on the tumor site by direct injection or intravenous injection. After, by heating the tumor tissue to 41 to 46ºC, the treatment will cause cancer cells apoptosis. MNPs have been used as heat generators in hyperthermia treatments since their magnetic properties allow them to transform magnetic energy into heat [5].

Taking advantage of the large number of applications, MNPs can also deliver the correspondent drug at the accurate point of the body to treat cancer tissues.

2.2.2. Drug delivery

For magnetic drug delivery, MNPs are generally injected into the bloodstream, and then magnets are used to concentrate them in the disease locations. The advantage is that the drugs can be delivered into specific cells by exerting an external field. It was found that there are three types of behaviors allowing researchers to determine the drug behavior, as many factors can influence it (blood convection, diffusion and extravasation, among others): velocity dominated, magnetic dominated, and boundary-layer formation [5].

The size, surface chemistry, and charge are particularly important to ensure that the nanoparticles can stay for a long time in circulation executing drug delivery [4].

It is believed that MNPs with sizes ranging from 10 to 100 nm are the most suitable for drug delivery applications. The lower threshold is based on the fact that particles smaller than 10 nm are easily removed by extravasation and renal clearance. The upper threshold is not well defined, however, some recent data suggest that nanoparticles in the range 50–100 nm are smaller than the spleen cut off (200 nm) and can penetrate into large tumors following systemic administration [4].

Doxorubicin (DOX) is an anthracycline antibiotic used for the treatment of a wide variety of tumor types. However, it presents lethal side effects on healthy cells too. The major mechanism of DOX activity is the inhibition of the topoisomerase II–DNA complex, causing DNA damage through intercalation into the DNA double helix. Also, DOX generates free radicals that cause damage to DNA and cell membranes. Although DOX is a very useful chemotherapy drug, its clinical application is limited by its side effects and drug resistance. To overcome these limitations, many new nanocarriers, such as liposomes, polymeric nanoparticles, and gold nanoparticles have garnered particular interest in recent years [9,10].

A study by R. O. Rodrigues et al. analyzed the drug loading efficiency (DLE) and drug loading capacity (DLC) using hydrophilic graphene-based yolk-shell magnetic nanoparticles to deliver DOX (GYSMNP@PF127). Different amounts of DOX were mixed with a fixed amount of MNPs. Also, the pH and temperature-dependent drug release was analyzed as well as its kinetics [8].

Table 1 shows the drug loading efficiency and drug loading capacity for the different initial concentrations of DOX between 50 and 500 μg/mL. The drug loading capacity increases with the increase of the initial DOX concentration. These results show the extraordinary capability of these MNP to load high contents of DOX on its high surface area [8].

***Table 1**: DLE and DLC on GYSMNP@PF127 at different initial DOX concentrations ($C_{DOX,0}$) in phosphate buffer pH7.4. Standard deviation of triplicate drug loading test (n=3)* [8].

$C_{DOX,0}$ (μg/mL)	50	100	200	300	400	500
DLC (μg/mg)	96.0±1.0	196.5±0.4	394.1±1.0	587.0±0.5	771.2±9.0	910.5±11.0
DLE (%)	96.0	98.3	98.5	97.8	96.4	91.1

The tumor microenvironment presents a weakly acidic pH value around 6.0-7.2, and between 4.5 and 5.5 at the tumor tissue. Those pH differences justified the development of pH-dependent nanocarriers. The pH values used in this study were 7.4, 6.0, and 4.5 corresponding respectively to the mimicked physiological pH, tumor microenvironment, and intracellular tumor endosome/lysosome pH conditions, either at 37ºC (physiological temperature) and 45ºC (hyperthermia temperature). The results obtained, shown in Fig. 2, reveals that the drug release takes place in two stages: a rapid DOX release in the first 8h followed by a slower rate release until 48h. The findings show that a very low amount of DOX was released at physiological pH conditions. The influence of pH conditions is higher than the influence of temperature, the DOX release increasing at low pH values and high temperatures [8].

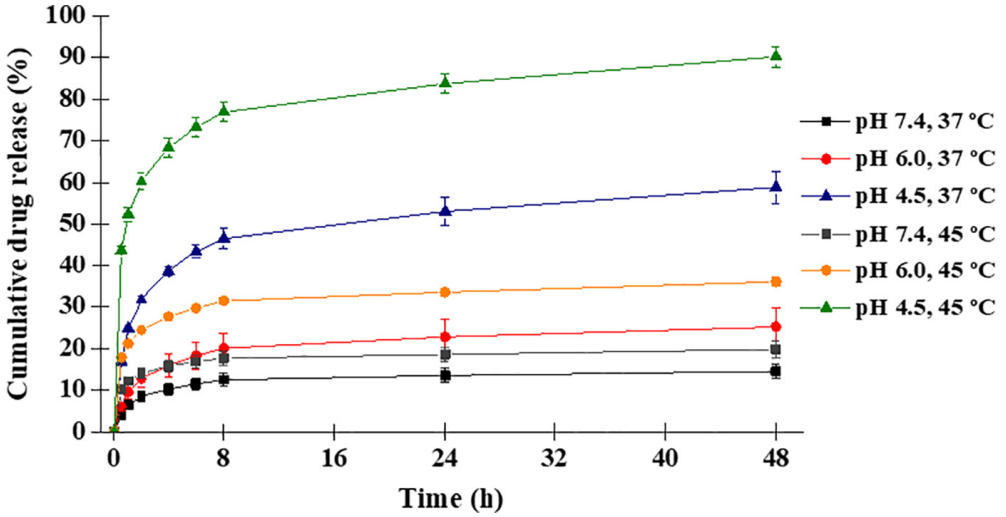

***Figure 2**: pH and thermo-responsive release of DOX from drug-loaded GYSMNP@PF127 under different pH values and temperatures. Standard deviation of triplicate drug release tests (n=3)* [8].

The results obtained, performed with the drug release data and the pH and temperature conditions mentioned before, were fitted to three kinetic models, namely first-order, Higuchi and Korsmeyer-Peppas. The model with the higher R^2 values (for each condition) was considered as the best model. The first-order and Higuchi kinetic models have very low R^2 values (slightly higher for the Higuchi model). These results suggest that the drug release, under the tested conditions, is not mainly concentration-dependent or totally controlled by diffusion behavior. The kinetic model that fits better is the Korsmeyer-Peppas model, as expected since it considers two parameters instead of one. The n values calculated from the Korsmeyer-Peppas model equation suggest that the drug release is essentially controlled by a simple quasi-Fickian diffusion mechanism [8].

A few authors have discussed the importance of mathematical models and endeavored to characterize drug release even if nanoparticulate dosage forms are complex and drug release evaluations are not straightforward. The use of mathematical models offers several advantages such as the elucidation of drug release mechanisms and guidance of the formulation development efforts or the representation and comparison of in vitro release profiles [9].

The control of release dosage forms enables pharmacists and engineers to work together with the aim of designing controlled drug delivery systems [10].

Zero-order and first-order kinetics can only fit in a few systems, therefore, in 1961, Higuchi described the first mathematical model to understand drug release. Some more investigations were done in the following years in order to improve the Higuchi model. The conclusions were that the amount of drug release depends not only on time and the initial amount of drug contained, but also on the solubility of the active agent in the matrix medium, the diffusion coefficient in the matrix medium, the porosity of the matrix, and on the capillary tortuosity factor [10,11].

2.2.3. Other applications

2.2.3.1. Magnetic resonance imaging (MRI)

MRI is one of the most powerful technique, not only for diagnostic radiology, but also for therapeutic medicine. Today, the rapid development of different kinds of imaging techniques, such as MRI, positron emission tomography, ultrasound and optical imaging are of great help for the early detection of diseases, to understand basic molecular aspects of living organisms and to the evaluation of medical treatment. Among the advantages of MRI, it can be highlighted the extreme imaging flexibility, the high patient acceptance,

the capability to evaluate anatomic and physiologic parameters, as well as the acquisition of unique clinical information. MRI is thus regarded as one of the most powerful diagnostic tools in the medical domain [5].

Historically, the clinical MRI studies first appeared in 1979. The first commercial scanner was produced in 1980 and, in 1985, magnets with a field strength of 1,5 T were already available for commercial clinical MRI systems. In the following 10 years, numerous researches were done to obtain faster gradient systems. Recent developments have confirmed that low citrate superparamagnetic iron oxide nanoparticle concentrations are good for sufficient contrast in MRI, important feature to cell viability and function in cell-based therapies [5].

2.2.3.2. Hard tissue repair

Nanotechnology has been applied to bone repair and to orthopedic and dental implants in the past decade. There have been in the market some micro/nanofabricated implantable products, such as micro/nano biochips, and nano-artificial bones. In the laboratory, experimental products such as coating materials, and bone repair materials have been also studied. It is expected new developments in the future [5].

2.2.3.3. Tissue engineering

Tissue engineering is a method of trying to successfully achieve tissue regeneration without damage. This approach generally includes three parts: the in vitro culture of autologous cells, the combination of the cells with three-dimensional (3D) biodegradable scaffolds, and promoting the reformation of their original structure [5].

2.2.3.4. Biosensors

A biosensor is essentially considered a device capable of transforming a biological event into an easily detected cell. MNPs are suitable to serve as platforms for biosensors since the surface of MNPs can be easily modified with numerous receptors, and MNPs can serve as ferromagnetic labels [5].

Different biosensors can detect different biological substances. MNPs and a two-marker recognition system are used to develop a sensitive biosensor based on surface plasmon resonance spectroscopy. The cytosensor has great potential for exploring new applications for the detection of a large number of separation products based on MNPs. Besides, the glucose sensor based on chemical oxidative polymerization of pyrrole at the surface of $ZnFe_2O_4$ nanoparticles showed good activity. They are sensitive to detect

glucose. A novel electrochemiluminescence glucose biosensor based on Fe_3O_4 nanoparticles has also been synthesized [5].

Many other kinds of biosensors have been studied. A novel fluorescence biosensor based on aptamer was developed to detect chloramphenicol. The fluorescence biosensor used aptamer conjugated MNPs for recognition and concentration elements. And the biosensor used upconversion nanoparticles as highly sensitive signal labels. Another one tried to reduce the interference from ascorbic acid during the detection of dopamine. It showed high sensitivity and selectivity, micromolar detection limit, high reproducibility, and easy preparation [5].

2.3. Design of nanoparticle structures

MNPs can be divided into metal oxides, pure metals, and magnetic nanocomposites. The most used in the biomedical field are iron, cobalt and nickel metal alloys, as well as iron oxide, and ferrites. Among them, iron oxide nanoparticles are the most studied because of their low toxicity profile [5].

Coating materials with good biocompatibility can stabilize MNPs in physiologic fluids and provide chemical functionalities for additional modifications. In addition, the variation of the sizes of the nanoparticles and the adjustment of the concentrations of soft and hard magnetic phases in the materials can improve their suitability for biomedical applications [5].

The preparation of macroscopic objects with a well-defined structure at the atomic or molecular level continues to be a very interesting subject, especially when working toward applications such as nanomedicine that have a critical need for well-defined structures. Molecular self-assembly is an approach to achieve this goal since in this approach engineered molecules or macromolecules, like building blocks, self-assemble in special routes to form different objects such as micelles, vesicles, ribbons, films, fibers, and tubules [12].

The nanostructures are usually developed considering a magnetic core covered with a metal or a non-metal structure (shell), such as gold, silica, and polymers, among others. In general, this core-shell approach allows protection of the magnetic core [13].

Metal nanoparticles can be synthesized by adopting physical or, chemical methods, such as photochemical reactions, thermal decomposition, electrochemical reactions and sonication. Most of the methods are related to certain disadvantages, such as using hazardous chemicals and high energy requirements which extended the environmental

toxicity and cost ineffectiveness. The biosynthetic method has been recognized as an environment-friendly, low-cost and safer alternative to chemical and physical methods. Nanoparticles can be synthesized from a variety of biological entities such as algae, bacteria, fungi, plants, viruses and yeast [14].

The current synthesis strategies for ordered mesoporous carbons (OMCs) are tedious and based on expensive non-renewable compounds. One of the most important challenges is to improve the sustainability of their synthesis and to find alternative precursors with less toxicity [15].

Research on iron oxide-based MNPs and their clinical use has been, so far, mainly focused on the spherical shape. However, it was demonstrated that cytotoxicity is size, shape, and dose-dependent. This means that different shapes should be studied. According to a study, the synthesis of elongate-shaped nanoparticles has been of major interest for drug delivery applications, owing to the superparamagnetic behavior, the control over drug-release profiles and biocompatibility. Furthermore, elongated nanoparticles can induce a stronger local magnetic field over a larger volume than spherical nanoparticles with equivalent volume, making them highly important as T2 contrast agents [16].

2.3.1. Composition

Different MNPs have been prepared using different compositions and phases, involving pure metals such as Fe, Co, Ti, and Ni, metal oxides such as Fe_3O_4 and γ-Fe_2O_3, ferrites such as $BaFe_{12}O_{19}$, $SrFe_{12}O_{19}$ and MFe_2O_4 (M corresponds to Cu, Ni, Mn, and Mg, among others) and metal alloys such as CoPt and FePt [17].

Highly magnetic-responsive materials, such as Co and Ni, are toxic and are liable to oxidation, which impedes their use in most biomedical applications. On the other hand, iron oxide NPs, namely magnetite (Fe_3O_4) and maghemite (γ-Fe_2O_3), are the most extensively studied and applied in the biomedical field, due to their biocompatibility, super-paramagnetic behavior and chemical stability at room temperature [17].

The most used MNPs on drug delivery systems are magnetite (Fe_3O_4) and maghemite (γ-Fe_2O_3). Such MNPs doped with particular drugs have some application problems, as stability and nontoxicity in the physiological media, not being easy to join high biocompatibility, magnetic saturation, and interactive functions on the magnetic nanoparticle surface. As a solution, the polymer coating not only allows the increase of

the hydrophobicity of the nanoparticle, but also offers a diversity of surface functional groups to bind drug molecules, increase stability and inhibit agglomeration [17].

2.3.2. Structures

Lately, the research on MNPs has been moving towards the directions of anisotropic shape, hollow, core-shell (CS), yolk-shell (YS), Janus, composite, and doped, among others, due to their higher surface area, improved functionalities, and other physicochemical properties against those of simple spherical particles [18].

When comparing CS and YS structures it is found that CS MNPs are mainly dependent on the sequence of core and shell, the sizes of each, and the combination of materials. On the other hand, YS is a hybrid structure consisting of a movable core inside the hollow shell of the same or different materials. The main difference between CS and YS structures is the presence of a void space in the YS structure, derived from a sacrificial layer inserted between the core and the shell. This gives to the YS structure a few specific advantages, such as the possibility to be synthesized from a single material to enhance the specific surface area, to provide more active sites, the suitability to accommodate guest molecules in the void space, and the higher active inner and outer surfaces provided by the shell layer and space for the expansion of core MNPs in many applications provided by the void space [18].

2.3.3. Types of YS MNPs

YS MNPs is a specific class of CS MNPs, where the presence of the void space makes them special [18].

YS MNPs can be classified into ‘spherical’ and ‘nonspherical’ structures. In the first case, both core and shell are spherical in shape, and in the second case at least the core or the shell should be non-spherical. In addition, spherical YS structures can be classified into five distinct subcategories: (a) single core/shell, (b) single-core/multi-shell, (c) multi-cores/single shell, (d) multi-cores/shells, and (e) multi-shells or shell in shell. The different types of spherical YS MNPs are shown in Fig. 3. Non-spherical YS NPs are also divided into two categories based on their geometry: complete non-spherical YS NPs, where both the core and the shell have a non-spherical shape, and partially non-spherical YS NPs, where either the core or the shell of the YS has a non-spherical shape [18].

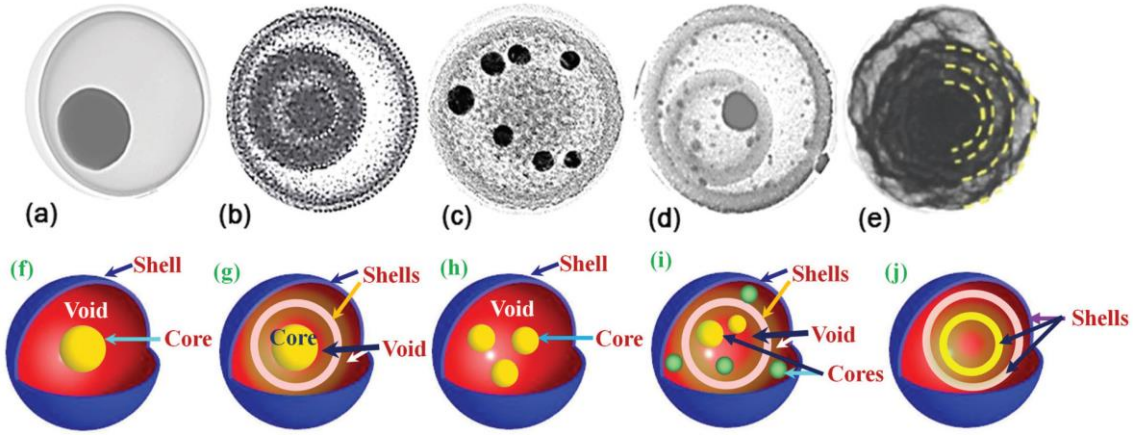

***Figure 3**: Different types of spherical YS MNPs (a) single core/shell, (b) single-core/multi-shell, (c) multi-cores/single shell, (d) multi-cores/shells, and (e) multi-shells or shell in shell [18].*

The single-core/shell is the simplest structure made of either the same or different materials for the core and the shell. They can be classified attending to the materials used (organic or inorganic). For biomedical applications, the type of core with a silica shell (inorganic/inorganic type) is interesting as it is simple to synthesize, it is chemically inert and non-toxic, among other advantages. A metallic shell can be interesting for optical and magnetic imaging. Also, metal oxide/polymer structures, where only Fe_3O_4 and SiO_2 metal oxide MNPs have been reported as core, are adequate for biomedical applications as they are thermo and pH-responsive, biocompatible, and allows the encapsulation of drugs [18].

Very little attention has been directed towards single-core/multishell YS MNPs. This type is complex but very important for different applications due to its very high specific surface area, abundant inner voids, and multiphase heterogeneous interfaces [18].

Multicores/single shell develops new physical and chemical properties as its structure leads to the encapsulation of the same or different multicore nanoparticles. Multicores of noble metals are mostly encapsulated in silica, carbon and metal oxide hollow shells. The different properties obtained make them useful for various applications such as drug delivery [18].

As the single-core/multishells and the multicores/single shell structures have much better properties than the single structures, it is also expected that multicore/multishell structures will provide additional multifunctionality. There is only one study reported so far related to the multicore/double-shell YS structure speculating biological applications with improved mechanical, optical, and other properties [18].

Multiple shells or shell in shell structure is defined as an encapsulation of hollow cores inside hollow shells. Considering drug delivery, this structure is extremely important due to the presence of high void spacing between the shells to encapsulate distinct drug and guest species [18].

2.4. Synthesis methods

2.4.1. Non-shelled MNPs

Different synthesis methods can be used to obtain MNPs, such as co-precipitation, hydrothermal synthesis, and sol-gel.

The co-precipitation method considers an aqueous precursor solution with stirring at a fixed temperature [19].

In the hydrothermal method, a clear metal-ion solution is formed. After a completely dissolved mixture, the solution is transferred to an autoclave, sealed, and maintained at high temperature [19].

The particle size obtained is highly different attending to the method used. For the manganese ferrite nanostructures formed by Leila et al., the highest particle size was obtained with the sol-gel synthesis, while the smallest particle size was obtained with the hydrothermal method. In addition, the magnetic properties seem to be affected by the synthesis method used [19].

The sol-gel method takes place in deionized water with stoichiometric amounts of the reagents. A neutral solution is expected before adding an acid, and then the mixture is slowly evaporated to form the gel [19].

The sol-gel method is one of the most useful and attractive technologies for the synthesis of ferrite MNPs because of its advantages, such as good stoichiometric control and the production of ultrafine particles with a narrow size distribution in a relatively short processing time at low temperature [20].

Sol-gel methods generally involve the hydrolysis and condensation of metal alkoxides or alkoxide precursors, leading to dispersions of oxide particles in a solution. The solution is then dried by solvent removal or chemical reaction. In general, water is used as the solvent, but the precursors can also be hydrolyzed by an acidic or basic medium. The catalysis process induces the formation of colloidal as well as the polymeric form of the gel [20].

The nonhydrolytic sol-gel routes have been emerging aiming at solving the problems faced in conventional aqueous sol-gel by a drastic change of the reactions and

the reaction medium. Although the reactions are typically slower than in aqueous media, this alternative provides control over the composition, structure, and texture of the resulting materials [21].

The characteristics of the final product depend on the rates of hydrolysis and condensation reactions. Smaller particles can be obtained at slower and more controlled hydrolysis rates. The solution composition, pH, and temperature have an influence on the particle size and also on the physical properties such as saturation magnetization, coercivity and remanent magnetization. The magnetic properties of the particles also depend on the phase, and volume fraction, being very sensitive to the size distribution and dispersion. The structural parameters and material porosity of the nanocomposites, derived from the gel can be determined by the rate of hydrolysis and condensation of the gel precursors as well as by other oxidation-reduction reactions that occur during the gelling and subsequent heat treatment stages [20].

Polyacrylic acid (PAA), citric acid, oxalic acid, and glycolic acid have been used as chelating agents in the sol-gel process to synthesize various spinel-type mixed oxides [20].

Iron carbides have excellent properties compared with iron or iron oxide nanoparticles since the carbon atoms occupying the interstices between close-packaged iron atoms. They show high saturation magnetization and low toxicity. The use of organic gelators to synthesize these materials made a remarkable advance. Small molecules, such as urea, or polymers as chitosan, have been employed to disperse soluble metal precursors within a homogeneous gel network. Upon heating in an inert atmosphere, the gel then decomposes and acts as a carbon source for carbide formation. It was found that melamine is particularly useful for this method due to the fact that it can be used to strongly bind and disperse metal precursors [22].

Xiaobai Wang et al. synthesized Fe_3C/C particles using melamine, CTAB and $FeCl_3 \cdot 6H_2O$ as starting materials. These materials were mixed before the reaction and in a process of water bath, the organic phase provides sites for metal cation binding. By dispersing the iron cations in the precursor within a functional gel, a stabilized homogeneous mixture of the precursor was formed. The proposal was that the occurrence of Fe_3O_4 and Fe as the intermediate phase in this mechanism could be rationalized by considering the microstructure and composition of the starting material. The organic phase simultaneously decomposed around these nanoparticles, producing a carbon-rich matrix. Finally, the core is Fe_3C and the shell is graphitic carbon. At the end, Fe_3C/C

MNPs were successfully synthesized. Varying the calcination temperature and heating rate, the average crystallite size obtained is different. It also affects the graphitization degree of the products. By changing the calcination time, the final products were tunable over a range of Fe_3O_4, Fe and Fe_3C [22].

2.4.2. YS MNPs

The approaches considered for the synthesis of YS MNPs are classified into two types: core-to-shell and shell-to-core. In the core-to-shell approach, the core is synthesized in a first step and then successively the shell layers. In the shell-to-core approach, the hollow shells are synthesized first and then the core nanoparticles are encapsulated inside the hollow shells [18].

The synthesis can be divided into four parts based on the method: sacrificial template-assisted synthesis, template-free approach, USP and the ship in bottle method [18].

The sacrificial template-based approaches have received great attention due to the simplicity of the process, easiness to retain the core shape and control over the void space. The generation of the void space can be differenced by three different types by the removal of the sacrificial layers. The first type is the complete removal of the sacrificial layer in which the sacrificial layer is made of different materials than the core and shell MNPs. The second type considers a partial dissolution of the core layer, where the core surface is partially etched after the formation of the core/shell structure. The last type involves the partial dissolution of the inner shell layer, where this layer is partially etched after the formation of the core/shell structure. It is easy to understand that the template removal or dissolution step is very important for the formation of the YS MNPs. At last, the sacrificial layer can be classified based on the physical states of the materials, as hard templates, soft types, galvanic replacement and Kirkendall reaction types [18].

The template-mediated synthesis methods have been used for several years to obtain MNPs with different sizes and shapes. Despite allowing to control different parameters adequately, in many cases the synthesis process requires several steps based on the complexity of the desired structure. On the other hand, removal of the sacrificial layer requires a few more steps, since in many cases it is made of some precious materials or they are environmentally harsh. Ostwald ripening is the physical method used in this case. In this process, small nanoparticles dissolve in solution and form large nanoparticles because of minimization of surface energy. A void space will be generated when the core is made of aggregates of small NPs and the shell is made of larger NPs. When the small

NPs are located at the central part of the spherical aggregates, it is called symmetric Ostwald ripening. On the opposite, if small nanoparticles are located asymmetrically on the spherical aggregates, then it is termed as an asymmetric Ostwald ripening process [18].

The ultrasonic spray pyrolysis (USP) method is a one-step, scalable and continuous approach. It is a solution-based process where high-frequency ultrasound is passed through the liquid precursor solution to generate a liquid-gas interface (aerosol), which is nebulized into micro-droplets. Finally, the generated droplets are carried by a gas flow into a furnace, where solvent evaporation and precursor decomposition take place to form the YS nanostructures. The volatile organic compounds form a layer at the NP surface and leave a void space to generate a YS structure during the heating process. The advantages of this method over conventional methods for the synthesis of YS structures includes the fact of being a one-step process, of not using acid or alkali treatments for dissolution of the sacrificial layer, of being an inexpensive continuous and environmentally friendly process with initial low-cost reactants and control on the composition [18].

The ship in a bottle approach is a simple approach where the precursor of the core material is encapsulated inside the pre-synthesized hollow shells and then the core particles are generated inside the hollow shells through a chemical reaction or by the self-assembly process to form a final YS structure [18].

2.4.3. Coating of non-shelled MNPs

Polymer network microgels are synthesized by free radical precipitation and inverse emulsion polymerizations [23].

In free radical precipitation, monomers, surfactant and cross-linker are initially mixed. Then, an initiator is added to give negatively charged free radicals. Free radicals can react with the oxygen of air and reagents of the reaction mixture. The reaction is carried out under a nitrogen atmosphere to avoid the possibility of consumption of radicals by oxygen. Therefore, the radicals react with monomers and cross-linker and produce a cross-linked polymer network. The morphology of the microgel particles and distribution of monomer units inside the polymer network depends on the time of addition of monomers into the reaction vessel. If all reagents are initially added, then they are incorporated homogeneously in the polymer network [23].

To carry out an inverse emulsion polymerization, the emulsifier is added into the organic phase. Monomers and cross-linkers are dissolved in an aqueous phase and then, the aqueous phase is added dropwise into an organic phase with constant stirring [23].

Three approaches can be considered towards the synthesis of microgels: mixing of dispersion method, growth of nanostructures in the presence of preformed microgels, and growth of microgel in the presence of preformed nanostructures [23].

When microgel dispersion is mixed with nanoparticle dispersion, then hybrid microgels are formed. Nanostructures may be symmetrically or asymmetrically distributed in the microgels depending on the method adopted for the mixing of dispersions [23].

For the growth of nanostructures in the presence of preformed microgels, the nanostructures are synthesized within preformed microgels, so they act as microreactors for the synthesis of nanostructures [23].

At last, for growing microgel in the presence of preformed nanostructures, the nanostructures should be initially prepared and then the polymer microgels are synthesized in the presence of these preformed nanostructures using the free radical precipitation [23].

2.5. Coating methods

Several synthesis routes have been developed to fabricate core-shell structures composed of a polymer and a carbon-coated magnetite, including the well-known "green chemistry" of the glucose hydrothermal process, the solvothermal process from organic iron compound (ferrocene) and hydrogen peroxide, the template method, and some other synthesis approaches. However, the core-shell products from these methods are always accompanied by aggregation of particles, and it is usually difficult to adjust the structural parameters of products through the control of the synthesis conditions. Therefore, developing a novel strategy to prepare well-dispersed and tunable core-shell magnetic carbon composites is still a challenge [24].

2.5.1. Formaldehyde and dihydroxybenzene resins

It is known that the base or acid-catalyzed resorcinol-formaldehyde (RF) reactions can form polymeric resins. Due to its common uses, its instability, and high costs, resorcinol in alternative is generally mixed with phenol-formaldehyde (PF) resol resin, obtaining the so-called phenol-resorcinol-formaldehyde (PRF) co-condensed resins [25].

A significant difference between PF and RF resins is that curing PF resins generally requires a hot-press temperature above 160ºC, whereas RF and PRF are cold-setting resins. This indicates that RF condensations encounter a much lower energy barrier and occur much faster [25].

Considering the structural similarity between the RF resin and silica gel, Liu et al. extended successfully the Stöber process used with the silica gel to the preparation of monodispersed RF polymer and carbon spheres, which simultaneously provided a new opportunity for the synthesis of RF and carbon-coated nanocomposites. For this process the MNP were dispersed in a solution of ethanol, followed by the addition of ammonia, resorcinol, and formaldehyde. The mixture was mechanically stirred at 30ºC for 24h. In addition, some TEOS as silica source was added to the reaction solution before the addition of the carbon sources. The final magnetic spheres were obtained by thermal treatment at 500ºC for 4h under a nitrogen atmosphere with a heating rate of 2ºC/min. The amount of the different compounds vary for the different polymer precursors [24].

2.5.2. Citric acid

Citric acid is a cheap and biocompatible compound that is used on a large scale in the food and drug industries. Despite the large-scale production and intrinsic importance of this substance, especially in biological systems, there are few reports on the production of polymeric materials based on it [12].

In ABA triblock copolymers of poly(citric acid) (PCA) and poly(ethylene glycol) (PEG) are synthesized and characterized. Molecular self-assembly of PCA-PEG-PCA copolymers in water led to the formation of different objects, from nanoparticles to fibers that were able to encapsulate fluorescein as a small guest molecule. Based on their molecular self-assembly, linear-dendritic PCA-PEG-PCA copolymers are promising nanomaterials to use in nanomedicine [12].

The toxicity and hemocompatibility of this polymer were investigated. According to the biocompatibility tests (crystal violet, hemolysis, LDH, and MTT assays), the toxicity of copolymers synthesized in 1 mg/mL or higher concentrations was considerable. Since self-assembly depends directly on the concentration of copolymers, it is probable that in high concentrations self-assembly is the main reason for the toxicity of the materials [12].

2.5.3. Plant and fruit extracts

The use of plant extracts in the synthesis of magnetic compounds have been explored due to their content in phenolic compounds. Polyphenols can reduce via green routes the iron ions to magnetite, enabling the formation of colloidal magnetic cores, by the incorporation of phenolic groups. Improved colloidal stability enables the individual coating of the magnetic nanomaterial into a single core-shell, avoiding the production of clusters of magnetite with carbon. Drug loading and release tests performed with CMNPs-plur revealed the ability to use this nanocomposite as pH-dependent drug nanocarriers. Impressively, the synthesized nanocomposite showed a drug loading of 99.1%. On the other hand, the final release was approximately 18% higher in the solution at mimicked acidic tumor environment than in a solution at pH equivalent to normal cells (physiological pH) [26].

A study with fruit extracts as the capping agent was done using strawberry, cherry, Malus Domestica, and Andean blackberry. Field emission scanning electron microscopy (FESEM) images show that the particle sizes of the nanocomposite prepared with strawberry are homogenously spherical, regular, and smaller than those produced by other capping agents. It has also the most promising role in the control of the morphology and particle size. The results obtained show that the extract of fruits as capping agent has an intense impact on the morphology and pore volume determination of the nanocomposite. Results of the study indicated that the as-prepared nanocomposite can be used as an effective carrier to drug delivery systems [27].

In another study, the purpose was to reduce iron III chlorides to iron nanoparticles by a biosynthesis method using Cinnamomum Verum extracts containing phenolic compounds that act as reducing and capping agents. The antioxidant, anti-inflammatory, and anti-diabetic assays showed the efficient behavior of Fe NPs with low concentration value in biomedical applications [14].

2.5.4. Phloroglucinol with glyoxylic acid

Glyoxylic acid is a plant-based compound that fits the idea of making the coating process more sustainable, rather than the widely employed and toxic formaldehyde. On the other hand, phloroglucinol is a fossil fuel derivative, and attempts to decrease its usage are highly desired, however, the phloroglucinol is a biocompatible compound and its toxicity is insignificant. Changing the resorcinol for the phloroglucinol, reduce the toxicity of the compounds involved in the process and a possible carcinogenic agent, as resorcinol is classified in group 3. [28], [29]

A balanced combination of lignin, phloroglucinol, and glyoxal, a less toxic version of glyoxylic acid, is proposed [15].

Studies performed by S. Herou et al. produced soft-templated carbons by carbonizing mixtures with different proportions of phloroglucinol and organosolv lignin, while maintaining constant the amount of both the cross-linking (glyoxal) and templating (F127 surfactant) agents. With the intention of comparison, three materials were synthesized denoted as (a) PG for phloroglucinol : glyoxal ([P] = 100 wt%); (b) PLG, from phloroglucinol : lignin : glyoxal ([L/P] = 50 wt%); (c) LG, from lignin : glyoxal ([L] = 100 wt%) [15].

In the selected solvent, acetone, the polypropylene oxide (PPO) units of F127 are expected to form the core of micelles while the polar groups of polyethylene oxide (PEO) protrude to interact with the solvent. When phloroglucinol is added to the solution, it self-assembles around PEO segments through hydrogen bonds. In analogy to cross-links generated from glyoxylic acid, upon thermal treatment (85 °C), glyoxal should act as a tetra-functional cross-linking precursor. Indeed, when the prepared mixtures were thermally treated, samples became insoluble and changed their physical characteristics: PG became a hard-thermoset resin and both LG and PLG turned into rubbery pastes, demonstrating the cross-linking ability of glyoxal in all systems. Well in agreement, thermogravimetric analysis (TGA) of crosslinked samples showed enhanced thermal stability when compared to their respective precursors. Interestingly, PLG and PG showed better thermal stability than LG. This might be attributed to the denser number of cross-links that can be generated when using a fixed amount of glyoxal concerning phloroglucinol and lignin. It is worth mentioning that the PLG material exhibits no significant decomposition before 400 °C. This might be due to a synergistic effect arising from improved crosslinking when both phloroglucinol and lignin are present [15].

As a result, the PLG material showed better electrochemical performance. Other characterizations are shown in table 2 [15].

***Table 2**: Electrodes characteristics for the materials presented* [15].

	Mass loading (mg/cm^2)	Thickness (μm)	Density calculated from PSD (g/cm^3)	Density calculated from thickness (g/cm^3)	Electrical conductivity (S/cm)	Cell resistance (Ω)

PG	6.7	100-110	0.73±0.02	0.62±0.02	0.7±0.1	0.62±0.01
PLG	10.2	115-120	0.98±0.02	0.87±0.02	0.9±0.1	0.41±0.01
LG	17.2	150-160	1.70±0.07	1.1±0.02	1.1±0.1	N.A.

Ordered mesoporous carbons (OMCs) through an environmentally friendly route, employing less toxic and bio-derived materials such as glyoxal and lignin were successfully prepared. Although the soft-templating methodology still relies on phloroglucinol usage, it was possible to retain an ordered porous structure by replacing half of the phloroglucinol with bio-derived lignin and still obtain a consistent cross-linking degree with glyoxal, without the need of any additional catalysts [15].

METHODOLOGY

3. Metodology

3.1. Reagents

The reagents used for the research were: Iron (III) chloride hexahydrate 99% ($FeCl_3 \cdot 6H_2O$, Aldrich), iron (II) chloride tetrahydrate ($FeCl_2 \cdot 4H_2O$, Aldrich), ammonia solution 28-30% (NH_4OH, Merck), phloroglucinol ($C_6H_6O_3$, Alpha Aesar), ethanol absolute 99.99% (C_2H_5OH, Fisher Chemical), pluronic F127 (Sigma Aldrich), glyoxal ($C_2H_2O_2$, Alpha Aesar), tetraethyl ortosilicate (TEOS, $SiC_8H_{20}O_4$, Fluka Chemika), sodium hydroxide 98.73% (NaOH, Fisher Chemical), nitric acid 37 wt% (HNO_3, Fisher Chemical), sodium dihydrogen phosphate monohydrate ($NaH_2PO_4 \cdot H_2O$, Pronalab), sodium hydrogen phosphate dehydrate (Na_2HPO_4 $2H_2O$, V.P.), distilled water, ultrapure water, doxorubicin (DOX, $C_{27}H_{29}NO_{11}$, Discovery Fine Chemicals) and omeprazol (OME, $C_{17}H_{19}N_3O_3S$, Acros Organics).

3.2. Synthesis of MNPs

For better understanding, the process of synthesis of the MNPs can be divided in the following steps:

Step 1 – Synthesis of magnetite core.

Step 2 – Coating process with a resin based on phloroglucinol.

Step 3 – Carbonization.

Step 4 – Etching with NaOH.

Step 5 – Nitric acid oxidation.

Step 6 – Functionalization with PF127.

From this point forward, the materials obtained will follow a naming compound by a letter and a number with the next meanings:

- A: Magnetic core (magnetite).
- B: Resin coated material.
- C: Carbonized material.
- D: Etched material with NaOH.
- E: Oxidized material with HNO_3.
- F: Functionalized material with PF-127.

- 1: Material synthesized using PF-127 during the coating.
- 2: Material synthesized without PF-127 during the coating.

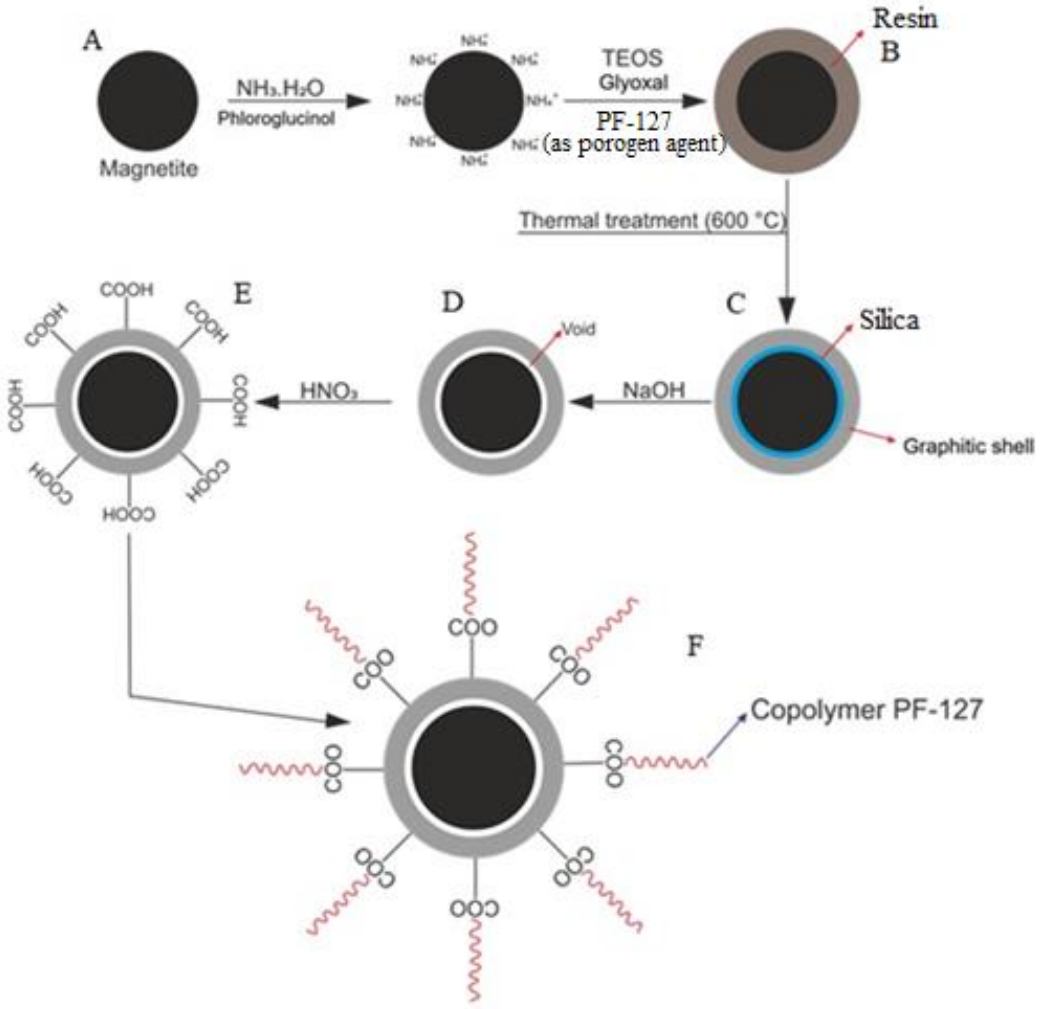

***Figure 4**: Materials obtained after each step of synthesis step*

3.2.1. Synthesis of magnetic core

The magnetic core, sample A, was synthesized by coprecipitation using iron (III) chloride hexahydrate and iron (II) chloride tetrahydrate as iron sources. A quantity of 0.53 g of $FeCl_2 \cdot 4H_2O$ (67 mM) and 1.11 g of $FeCl_3 \cdot 6H_2O$ (134 mM) are dissolved in 100 mL of distilled water in a two-neck round-bottom flask. The vessel containing this solution is heated using an oil bath to 55 ºC. Once this temperature is achieved, an ammonium hydroxide solution 1 M is dropped into the flask using a peristaltic pump until reaching a pH equal to 9. Once the pH value is confirmed, the solution stays under magnetic stirring at the same temperature for 30 min.

Finally, the material is washed with distilled water until reaching neutral pH, recovered with ethanol, and dried overnight at 60 ºC.

3.2.2. Coating process

A suspension with 0.25 g of MNPs and 50 mL of distilled water is prepared in an Erlenmeyer flask and mixed in an ultrasonic bath for 30 min.

During this step in a one pot strategy the magnetic core covered with a resin is obtained (sample B). In this work, one sample was prepared considering the formation of the resin in the presence of FP-127 and a second sample in which the core was coated in the absence of PF-127 as porogen agent, as descrived in the following:

Using PF-127:

The MNPs suspension is transferred to a 250 mL two-necked round-bottom flask previously loaded with 0.20 g of PF127, 0.10 g of phloroglucinol, 1.2 mL of ammonia 30 w% and 150 mL of ethanol.

The mixture is then heated at 30 ºC, remaining at this temperature for 1 h. After this time 0.10 mL of glyoxal 40 w% and 0.21 mL of TEOS are added dropwise with a micropipette and the mixture is maintained under stirring for 6 h at 30 ºC. Finally, the solution is heated at 80 ºC and maintained for 8 h under constant stirring.

The resultant product is washed with deionized water until reaching pH 7, recovered with ethanol and dried overnight at 60 ºC, resulting in sample B1.

Without PF-127:

The MNPs suspension is transferred to a 250 mL two-necked round-bottom flask previously loaded with 0.10 g of phloroglucinol, 1.2 mL of ammonia 30 w% and 150 mL of ethanol.

As in the previous process, the mixture is heated at 30 ºC, remaining at this temperature for 1 h. After this time 0.10 mL of glyoxal 40 w% and 0.21 mL of TEOS are added dropwise with a micropipette and the mixture is maintained stirred for 6 h at 30 ºC. Finally, the solution is heated at 80 ºC and maintained for 8 h under constant stirring.

The resulted product is washed with deionized water until reaching pH 7, recovered with ethanol and dried overnight at 60 ºC, resulting in sample B2.

3.2.3. Carbonization

The product obtained in the previous step is carbonized in a vertical tubular furnace. The gas-phase thermal treatment occurs under an N_2 flow of 100 $N \cdot cm^3$/min. It is heated to 120 and 400 ºC, staying 1 h at each temperature and then at 600 ºC for 3 h using a heating rate of 2 ºC/min in each temperature ramp.

During this step is expected the formation of the silica and a graphitic shell due to the thermal treatment applied to the resin previously obtained, yielding samples C1 and C2, when PF-127 is used or not used, respectively.

3.2.4. Etching with NaOH

The MNPs obtained in the previous step are etched under magnetic stirring with a 10 M sodium hydroxide solution for 16 h at room temperature. 1 mL of the solution is used for 10 mg of MNPs.

The resultant product is washed with deionized water until reaching pH 7, recovered with ethanol and dried overnight at 60 ºC.

After the etching a void will appear due to the removal of the silica formed in the previous step. At this point a yolk-shell structure will be obtained, yielding samples D1 and D2, when PF-127 is used or not used, respectively.

In Figure 5 is shown the set up used for drop the NaOH solution into the MNPs suspension to carry out the etching step.

Figure 5: *System used to drop the NaOH solution into the MNPs suspension*

3.2.5. Nitric acid oxidation

The MNPs are treated with nitric acid 1 M in a round bottom flask under magnetic stirring at 65 ºC for 3 h (1 mL of the solution is used for 5 mg of MNPs).

The resultant product is washed with deionized water until reaching pH 7, recovered with ethanol and dried overnight at 60 ºC, resulting in samples E1 and E2, when PF-127 is used or not used, respectively.

3.2.6. Functionalization with Pluronic F127 ®

The MNPs (2 mg/mL) are functionalized with PF127 (40 mg/mL) staying for 5 h under magnetic stirring at room temperature.

The product is washed to remove the copolymer by centrifugation at 13000 rpm for 20 minutes. The recovered MNPs stay suspended in water at a concentration of 10 mg/mL, resulting in the samples F1 and F2, when PF-127 is used or not used, respectively.

This step along with the nitric acid treatment form the hydrophilization of the particle, which would make the MNPs more stable in water and with biocompatibility characteristics.

3.3. Characterization

To characterize the MNPs, their porosity, structure and magnetic properties, porosimetry, transmission electron microscopy (TEM) and magnetometer techniques were used.

XRD analysis:

The measurements of powder XRD are obtained on a diffractometer DRON-3 by depositing the material in the glass sample holder, which allows to identify the type of metallic particle for the iron catalyst. Consequently, the XRD pattern is the fingerprint of the periodic atomic arrangements in a given material.

FT-IR analysis:

The Fourier Transform Infrared Spectroscopy (FT-IR) spectra of the different samples is recorded on a Perkin Elmer FT-IR spectrophotometer UATR Two infrared spectrophotometer, with a resolution of 4 cm^{-1}, to observe the bands related to vibrations of bonds or atoms present in a sample. The range of wavenumber covered is from 450 cm^{-1} to 4000 cm^{-1}. All the measurements are done at room temperature using CNT with non-additional treatments (in solid state). This analysis was performed at the Analytical Chemistry Laboratory of the Bragança Polytechnic Institute (IPB).

3.4. Drug loading

PBS pH 7.4 is prepared with 95 mL of $NaH_2PO_4 \cdot H_2O$ 0.2 M and 405mL of $Na_2HPO_4 \cdot 2H_2O$ 0.2 M.

The determination of DLC and DLE was then studied considering two different drugs: DOX and OME.

For the drug loading a solution of 500 μg/mL of each drug are prepared with the PBS 7.4. The drug loading is conducted by adding 20 mL of the drug solution and 20 mL of functionalized MNPs with a concentration of 1 mg/mL in the same PBS. The mixture stays in an orbital shaker for 48 h at room temperature. The drug-loaded material is lyophilized and stored in a freezer.

The drug concentration at the end of the drug loading process is determined by spectrophotometry.

The measure of a negative control and three different loadings are considered.

Once the calibration curve is calculated and the concentrations are obtained, the DLC and DLE are calculated by equations 1 and 2:

$$DLC = \frac{C_{NC} - C_f}{C_{NC}} \quad [1]$$

$$DLE = \frac{C_{NC} - C_f}{C_{NC}} \; x\, 100 \quad [2]$$

Where C_{NC} is the concentration calculated for the negative control (just the drug) and C_f is the final measured concentration of the drug.

Figure 6 shows the orbital shaker where the drug loading process takes place.

Figure 6: *System used to carry out the drug loading experiments*

3.5. Drug release

Drug release tests were performed in different solutions: PBS pH 4.5, PBS pH 6.0 and PBS pH 7.4.

To prepare PBS pH 4.5, 3.40g of $NaH_2PO_4 \cdot H_2O$ are diluted in 500mL of ultrapure water. For PBS pH 6.0, 24.6mL of $Na_2HPO_4 \cdot 2H_2O$ 0.2M are mixed with 175.4mL of $NaH_2PO_4 \cdot H_2O$ 0.2M.

To carry out the drug release tests, 2mg of the lyophilized drug loaded material are added to 20mL of each PBS. The liquid is collected and refilled at the selected time intervals (0.5, 1, 2, 3, 4, 6, 24 and 48 h). The absorbance of the samples is measured to determine the drug release extent. The experimental system used to carry out the drug release is shown in Figure 7. This equipment enables the control of temperature during the drug release tests.

The concentrations were determined by spectrophotometry (T70-UV-VIS) at 480 nm for DOX and 300 nm for OME.

The concentrations were calculated in μg/mL by a calibration curve previously determined. Once all the concentrations are calculated the percentage released can be obtained by equation 3:

$$\%released = \frac{C_m}{C_0}\ x\ 100 \qquad [3]$$

Where C_m is the measured concentration of the drug in the liquid for each selected interval time and C_0 the initial concentration of the drug loaded at the MNPs.

This calculation should be done for each time, where the initial concentration will vary, adjusting the value to the final concentration of drug remaining in the MNPs after the previous measurement.

To obtain the cumulative percentage released, which indicates the total drug released at each time, each percentage released at each time should be added.

***Figure 7**: System used to carry out the drug release tests*

RESULTS AND DISCUSSION

4. Results and discussion

4.1. Synthesis of the MNPs

In Table 3 are summarized the values of mass treated and recovered after each step of the MNPs synthesis:

***Table 3**: Mass treated and recovered after the different steps during the synthesis of the MNPs. M1: material obtained using PF-127; M2: material obtained without PF-127*

Step	Coating	Carbonization	Etching	Hydrophilization
Mass treated M1 (g)	2.00	2.37	1.81	1.28
Mass recovered M1 (g)	2.37	1.95	1.45	0.185
Gain (+) or loss (-) in g	+0.37	-0.42	-0.36	-1.095
Mass treated M2 (g)	2.25	2.52	2.16	1.45
Mass recovered M2 (g)	2.52	2.19	1.60	0.192
Gain (+) or loss (-) in g	+0.27	-0.33	-0.56	-1.258

As shown in Table 3, there are significant mass losses during the process, particularly in the etching and hydrophilization steps. Even observing that there is a gain of mass after the coating step, the final recovered mass is lower than 10% of the initial magnetite treated in both synthesized MNPs. These losses can occur by different reasons and in some steps loss of mass is already expected, as in the etching, where the goal is to remove the silica from the particle. In other steps, some material can stay emprisioned to the different equipment used, or even sent away during the washing step.

Following the methodology, the coating is started once a minimum of 2 g of the magnetic core (sample A) was recovered. During the coating step, as expected, the mass increases, which can be attributed to the formation of the coating. An increment of 18.5% and 12% for B1 and B2 respectively were obtained in this study. The differences of the increase can be related to the washing efficacy, as some product can be lost with the washing liquid.

At the carbonization step the first losses emerge. At this point the losses are reasonable, 17.72% and 13.10% for the recovering of C1 and C2 respectively.

During the etching step bigger losses appear representing a total loss of 19.89% and 25.93% of the initial mass for D1 and D2 respectively. As explained before, this is expected, due to the removal of the resin.

The hydrophilization step is the most costly process. The results show mass losses of 85.55% and 86.76% for F1 and F2 respectively. Due to the stability in water expected for the final material, the losses can be attributed to the difficulty involved in the washing process.

4.2. Characterization

4.2.1. X-ray diffranction

X-ray diffraction (XRD) was used to characterize the crystallography of the magnetic core of the obtained MNPs. The XRD spectrum is presented in Figure 8 and shows characteristic peaks at 30.24º, 35.73º, 43.36º, 53.79º, 57.36º and 63.02º, corresponding to magnetite nanoparticles [30].

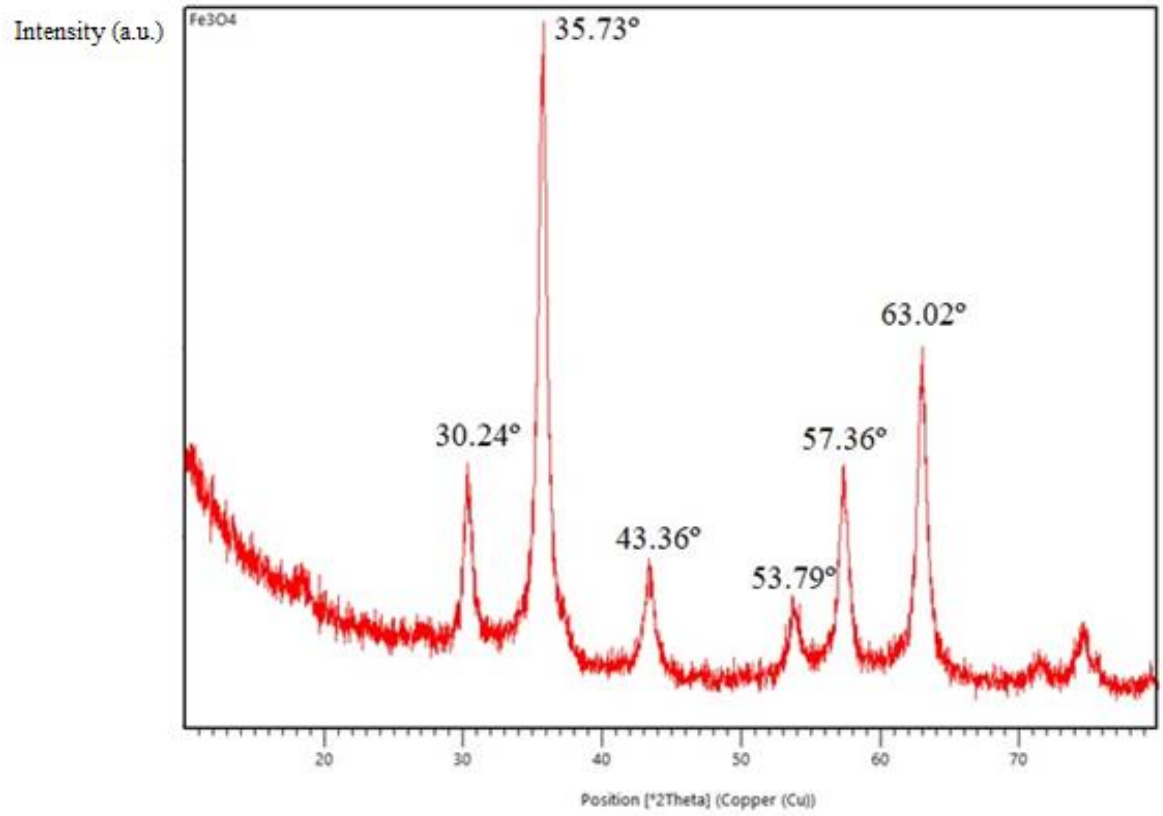

***Figure 8**: XRD patterns of the magnetic core*

4.2.2. FT-IR

The spectral analysis obtained by FT-IR, Figures 9 and 10, shows the comparison of the spectra of the nanocomposites in the different steps of the synthesis.

It is observed that the spectra are quite similar among the different materials and steps of the process.

The presence of magnetite is noticed in the absorption bands of 564 cm^{-1}, which corresponds to the vibration of the Fe-O bond. Bands at 1628 cm^{-1} and 3433 cm^{-1} are attributed to the bending and stretching vibrations of the surface –OH groups present in Fe [31].

These bands are present in all samples evaluated, meaning that magnetite is present in all of them, since it is the magnetic core.

The absorption bands at 1380 cm^{-1}, 1458 cm^{-1}, 1627 cm^{-1}, 2923 cm^{-1} and 3433 cm^{-1} represent the C-O, O-H, C=O, C-H and O-H bonds respectively, indicating that there are carboxylic acid groups in the samples. The presence of carboxyl's groups in the nanocomposites can improve the colloidal stability and monodispersibility in aqueous solutions. [28,29]

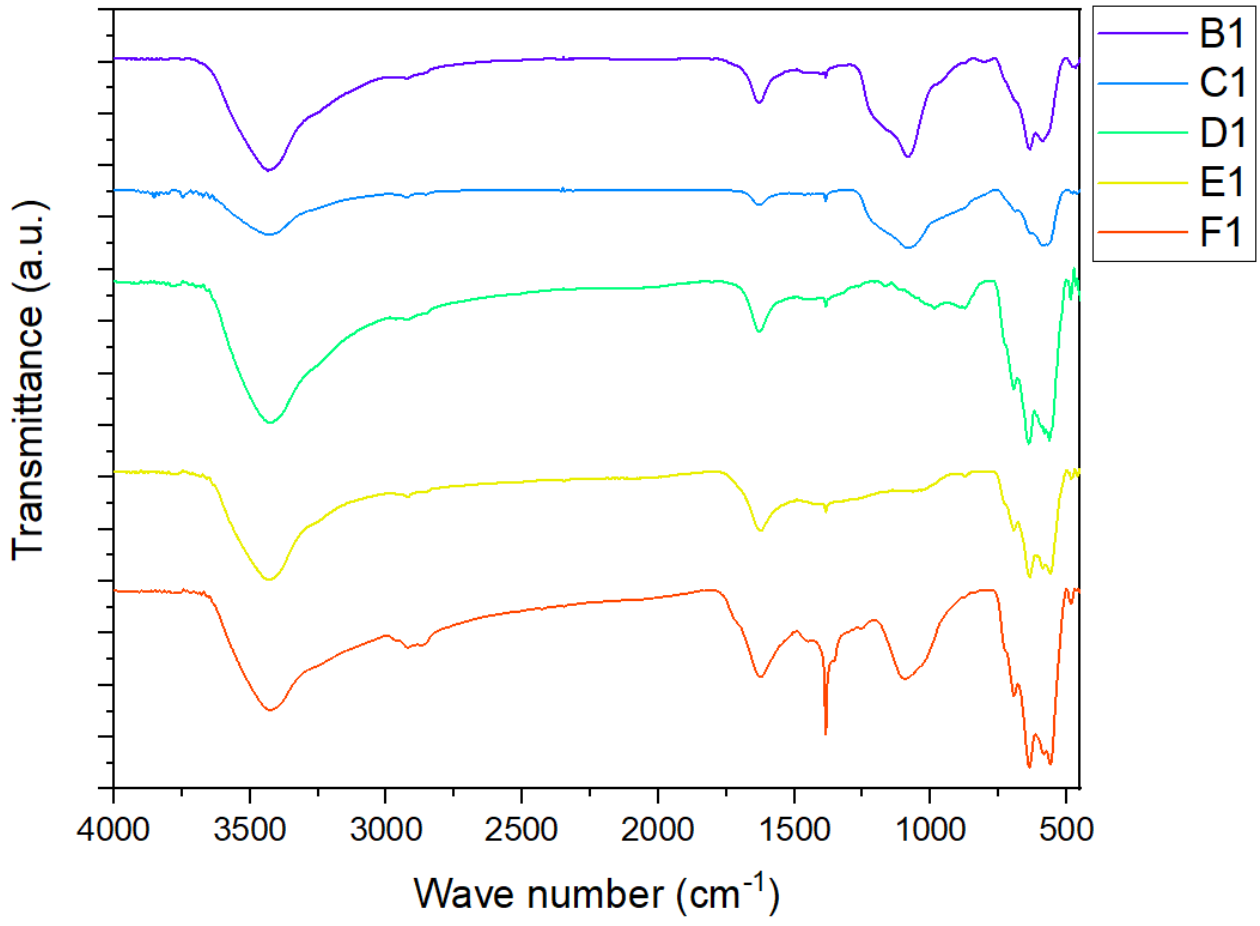

***Figure 9**: Absorption bands of the composites obtained in the different step of the synthesis using PF-127.*

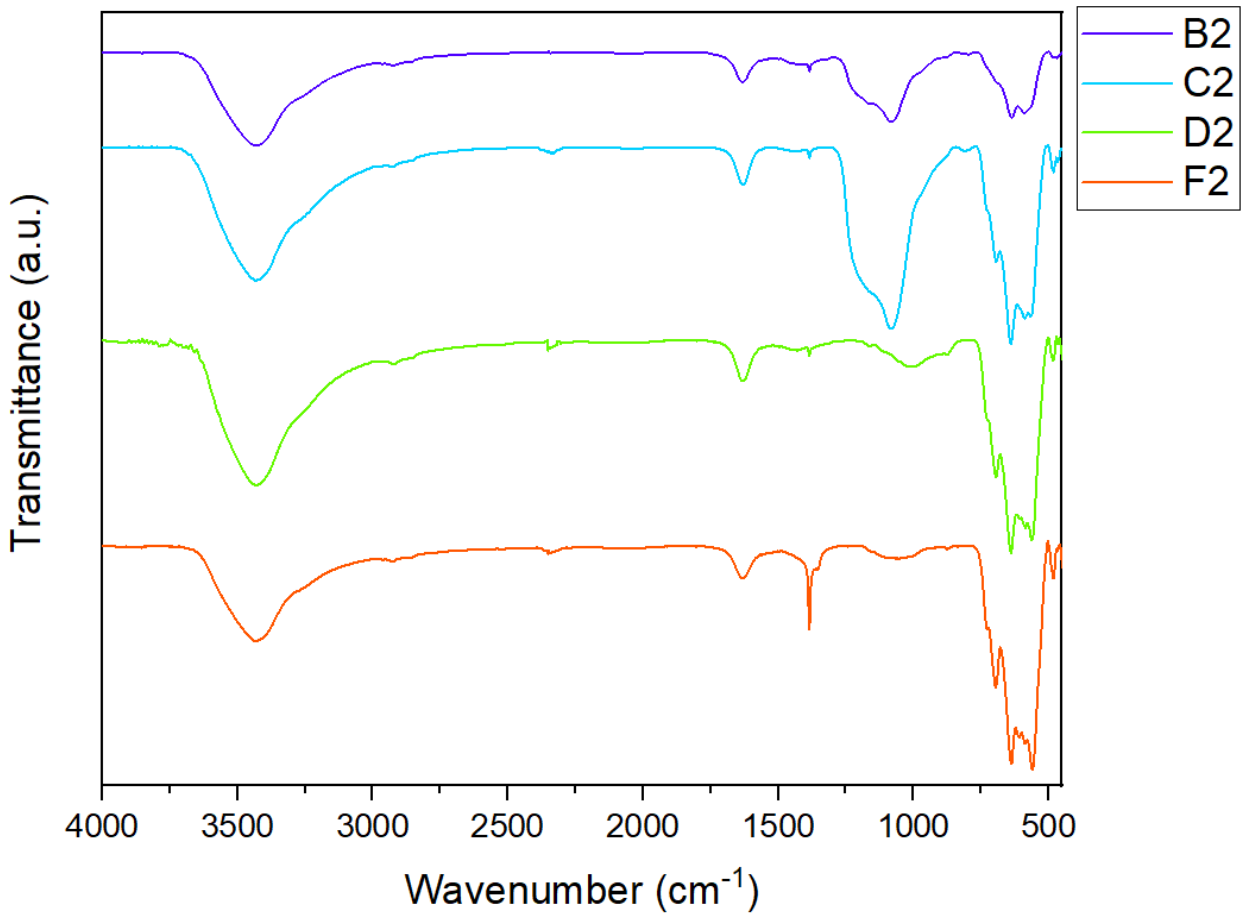

***Figure 10**: Absorption bands of the composites obtained in the different step of the synthesis without using PF-127.*

Comparing the results shown in Figures 9 and 10 the presence of the void generated after the etching is confirmed, by the band appearing at 1380 cm^{-1}, further disappearing in the sample after etching (samples D1 and D2), band due to the C-O. This band is supposed to reappear when the MNPs are hydrophilizated, as it is expected to obtain particles surrounded COOH groups. The band is just appearing again later in material F1. That can explain the instability in water of the second material (F2) as a fail in the last synthesis step.

4.3. Appearance of the MNPs

Visual differences were found between material 1 and material 2. The colour of the product obtained after carbonization was different for samples C1 and C2.

Once obtained sample F1, certain characteristics were observed. A black, magnetic, stable material, was obtained and ready for drug loading and delivery tests.

For the material synthesized without PF-127 as porogen agent, the colour observed after carbonization (sample C2) was different. The material become red, as shown in Figure 11.

***Figure 11**: Sample C2*

The colour indicates that material C1 probably gave rise to a graphitic shell after carbonization, while for material C2 a different product has emerged.

In Figure 12 it is shown the sample F2 suspended on water. It is observed that the material is not stable in water, as after 30 min almost all the material was precipitated.

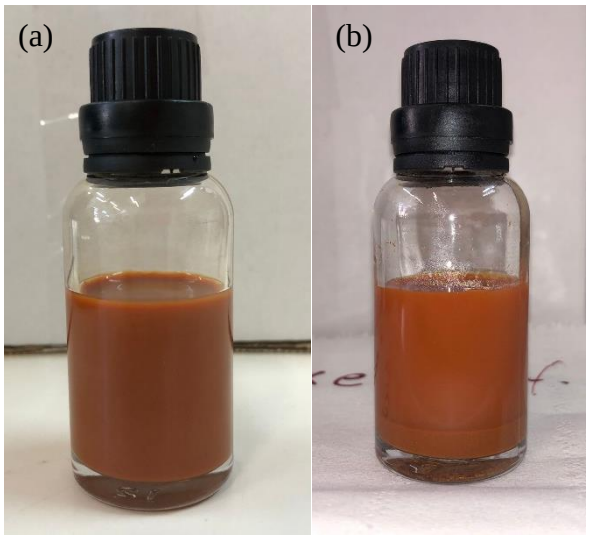

***Figure 12**: (a) Material F2 suspended on water. (b) Material F2 precipitated after 30 min.*

The instability of material F2 might be due to its wrong composition. It is expected that the reaction between nitric acid and the graphitic shell will increase carboxylic groups, fundamental for the functionalization with pluronic. As the red colour actually indicates that the graphitic shell was not obtained, it will not be able to form bonds with pluronic, the functionalization not being achieved, and the material not becoming stable.

4.4. Drug loading capacity and drug loading efficiency

As explained above, the material F2 was not stable in water, which make the material useless for biomedical applications. Accordingly, the drug loading and release tests with the drugs DOX and OME were carried out just with material F1.

To load the drugs into the MNPs, a PBS pH 7.4 medium was used. The results of DLC and DLE are shown in Table 4.

***Table 4**: Results of drug loading capacity (DLC) and drug loading efficiency (DLE) obtained for sample F1.*

Drug	DLC (mg/mg)	DLE (%)
DOX	0.9876	98.76
OME	0.3635	36.35

From Table 4 it is observed that 0.9876 mg of DOX were loaded in 1 mg of MNPs, which imply a DLE of 98.76%.

In the case of loading OME, the result was significantly lower, only 0.3635 mg of the drug being loaded in 1 mg of MNPs, wich is translated into a DLE of 36.35%.

These results are considerably better than previous results obtained with other materials in the research group where this work was carried out. The DLE results obtained for the same magnetic core, following coating by Solution Combustion Synthesis, using citric acid and tangerine peel extract for the reduction of Fe (III), as two different approaches, were 93.6% for DOX and 33.5% for OME [30].

The difference of the DLE between the DOX and OME drugs can be explained with their cation characterization. The MNPs are obtained in a cation form. The DOX exist almost entirely in the cation form in the environment, while the OME exist partially in cation form. This difference can explain a better affinity to the MNPs of the DOX. [33], [34]

4.5. Effect of pH on drug release

The pH-dependence release seems interesting to study due to the differences between the pH in the tumor and the physiological pH. The normal tissues have a pH value of 7.4, while the pH of intracellular tumor tissues is 4.5. A pH value of 6.0 will correspond to the tumor microenvironment. A pH-sensitive drug delivery nanocarrier is interesting to improve the drug release into the tumor tissues and to avoid side effects in the healthy cells. Accordingly high drug release values are desired in acidic mediums for the studies performed. This effect is impulsed by the chemistry behind the bond between the material and the drug.

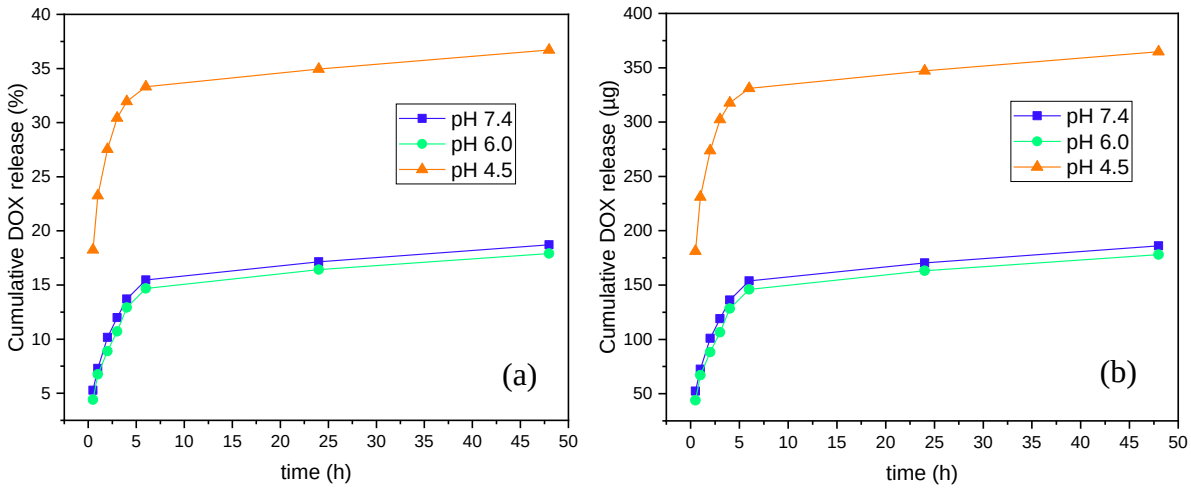

***Figure 13**: (a) Cumulative release of DOX (%). (b) Cumulative release of DOX (µg). (The line was printed as a view guide)*

Figure 13 shows the DOX release at different pH values in mass percentage (a) and in total mass (b). As shown in Figure 13, the drug release percentages reached after 48h of drug release are 18.71%, 17.91% and 36.72% for PBS solutions at pH 7.4, 6.0 and 4.5, respectively. These results can also be expressed in weight DOX quantities of 185.97 µg, 177.96 µg and 364.87 µg for PBS solutions at pH 7.4, 6.0 and 4.5, respectively (from the loaded 993.75 µg).

As desired, the largest amount of DOX is released in the acidic medium. The result obtained at pH 7.4 is slightly higher than a pH 6.0. This can be due to the pH of zero charge of the material, which can cause a higher liberation at its pH.

Comparing with previous studies, the maximum released achived is slightly smaller. 39.33% of DOX, representing a weight of 516.97 µg, were released in a work carried out in the research group where this work was developed, using different approaches for the coating of MNPs. In addition, the results obtained in that work revealed a larger difference of release between pH values (29.05% and 7.10% at pH 6.0 and 7.4, respectively), which represents a more interesting result for the desired applications [30].

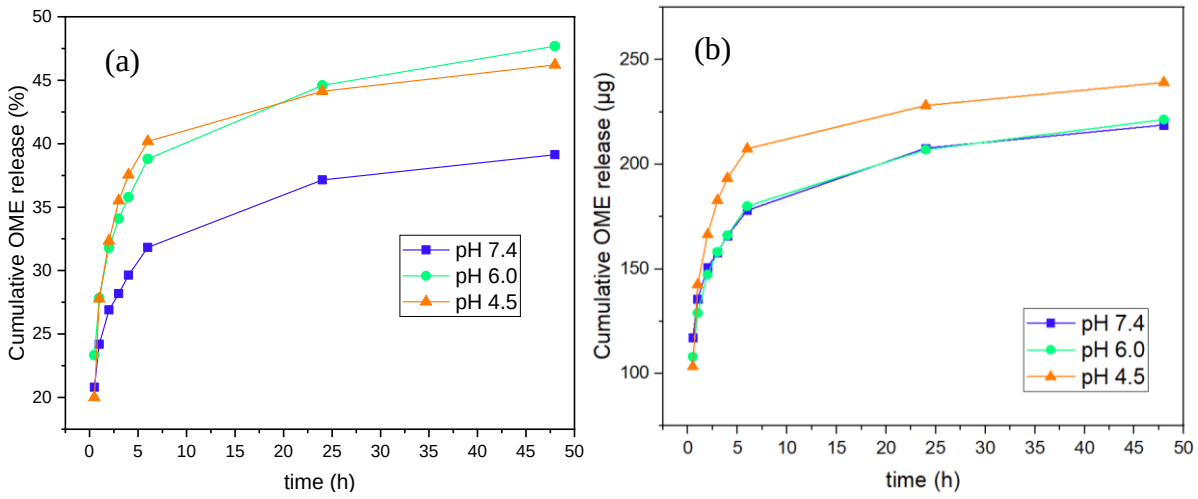

***Figure 14**: (a) Cumulative release of OME (%). (b) Cumulative release of OME (µg). (The line was printed as a view guide)*

Figure 14 shows the release of OME at different pH values in mass percentage (a) and total mass (b). As shown in Figure 14, the drug release percentages reached after 48h of drug release are 39.12%, 47.68% and 46.21% for PBS solutions at pH 7.4, 6.0 and 4.5, respectively. These results can also be expressed in weight OME quantities of 218.81 µg,

221.39 µg and 239.18 µg for PBS solutions at pH 7.4, 6.0 and 4.5, respectively (from the loaded 527.16 µg).

In the case of OME, the result obtained in previous studies carried out in the research group where this work was developed, were not as desired, as the release was higher for higher pH values. The result obtained at this work has an improvement, as the release is higher at low pH values. Since as OME is used in the treatment of ulcers and gastroesophageal reflux disease which involve an acidic pH, it seems to have obtained more interesting results [30].

CONCLUSIONS AND FUTURE RESEARCH

5. Conclusions and future research

5.1. Conclusions

Related to the new carbon coating method, the results obtained shows the suitability of the resultant materials to the characteristics required (magnetic properties, sustainable coating, biocompatibility and stability in water). The characterization of the MNPs confirms the desired characteristics, as the magnetic properties and the capacity to load drugs for biomedical applications.

The results obtained for drug loading and drug release were satisfactory when DOX was considered. A DLE of 98.76% was obtained with a release after 48h of 18.71%, 17.91% and 36.72% for PBS solutions at pH 7.4, 6.0 and 4.5, respectively. The drug loading capacity was higher than in other studies and, as desired, the drug release tests revealed a better affinity with acidic medium. Compared with results previously obtained by the research group where this work was carried out, both DLC and drug delivery tests obtained better results.

The results obtained for drug loading and drug release using OME showed a progress comparing with other studies. The DLE obtained was a 36.35%, and the release after 48h of the drug loaded were 39.12%, 47.68% and 46.21% for PBS solutions at pH 7.4, 6.0 and 4.5, respectively. Even the results obtained in this work are quite low, they are higher than those obtained in previous researches and, as improvement, it shows better affinity with acidic mediums.

5.2. Future research

It would be interesting to get further insights about the unexpected results obtained in the particle synthesized without PF-127.

In order to guarantee the biocompatibility of the MNPs, it will be interesting to make some toxicity tests.

For drug loading improvement, the low amount of OME loaded in these tests should be analyzed, and the drug loading conditions adequated.

Finally, a thermo-response release could be investigated to simulate better the tumor tissue conditions.

REFERENCES

References

[1] M. R. Ibarra, C. Marquina, and J. G. Valdivia, "' Biomedical applications of magnetic nanoparticles I : Drug delivery ,'" pp. 1–5.

[2] S. H. Bossmann and H. Wang, Magnetic Nanomaterials: Applications in Catalysis and Life Sciences. Royal Society of Chemistry, 2017.

[3] M. Tadic, S. Kralj, M. Jagodic, D. Hanzel, and D. Makovec, "Magnetic properties of novel superparamagnetic iron oxide nanoclusters and their peculiarity under annealing treatment," Appl. Surf. Sci., vol. 322, pp. 255–264, 2014, doi: 10.1016/j.apsusc.2014.09.181.

[4] N. Tran and T. J. Webster, "Magnetic nanoparticles: Biomedical applications and challenges," J. Mater. Chem., vol. 20, no. 40, pp. 8760–8767, 2010, doi: 10.1039/c0jm00994f.

[5] X. Li et al., "Current investigations into magnetic nanoparticles for biomedical applications," J. Biomed. Mater. Res. - Part A, vol. 104, no. 5, pp. 1285–1296, 2016, doi: 10.1002/jbm.a.35654.

[6] W. Wu, Z. Wu, T. Yu, C. Jiang, and W. S. Kim, "Recent progress on magnetic iron oxide nanoparticles: Synthesis, surface functional strategies and biomedical applications," Sci. Technol. Adv. Mater., vol. 16, no. 2, p. 23501, 2015, doi: 10.1088/1468-6996/16/2/023501.

[7] M. Pakdel, H. Raissi, and M. Shahabi, "Predicting doxorubicin drug delivery by single-walled carbon nanotube through cell membrane in the absence and presence of nicotine molecules: a molecular dynamics simulation study," J. Biomol. Struct. Dyn., vol. 38, no. 5, pp. 1488–1498, 2020, doi: 10.1080/07391102.2019.1611474.

[8] R. O. Rodrigues et al., "Multifunctional graphene-based magnetic nanocarriers for combined hyperthermia and dual stimuli-responsive drug delivery," Mater. Sci. Eng. C, vol. 93, no. November 2017, pp. 206–217, 2018, doi: 10.1016/j.msec.2018.07.060.

[9] S. D'Souza, " A Review of In Vitro Drug Release Test Methods for Nano-Sized

Dosage Forms ," Adv. Pharm., vol. 2014, pp. 1–12, 2014, doi: 10.1155/2014/304757.

[10] "Mathematical models of drug release," Strateg. to Modify Drug Release from Pharm. Syst., pp. 63–86, 2015, doi: 10.1016/b978-0-08-100092-2.00005-9.

[11] C. Mircioiu et al., "Mathematical modeling of release kinetics from supramolecular drug delivery systems," Pharmaceutics, vol. 11, no. 3, 2019, doi: 10.3390/pharmaceutics11030140.

[12] A. T. Naeini, M. Adeli, and M. Vossoughi, "Poly(citric acid)-block-poly(ethylene glycol) copolymers-new biocompatible hybrid materials for nanomedicine," Nanomedicine Nanotechnology, Biol. Med., vol. 6, no. 4, pp. 556–562, 2010, doi: 10.1016/j.nano.2009.11.008.

[13] R. Rodrigues et al., "A Tailor-Made Protocol to Synthesize Yolk-Shell Graphene-Based Magnetic Nanoparticles for Nanomedicine," C, vol. 4, no. 4, p. 55, 2018, doi: 10.3390/c4040055.

[14] M. Sivakami, K. Renuka Devi, R. Renuka, and T. Thilagavathi, "Green synthesis of magnetic nanoparticles via Cinnamomum verum bark extract for biological application," J. Environ. Chem. Eng., vol. 8, no. 5, p. 104420, 2020, doi: 10.1016/j.jece.2020.104420.

[15] S. Herou et al., "Ordered mesoporous carbons from lignin: A new class of biobased electrodes for supercapacitors," Green Chem., vol. 21, no. 3, pp. 550–559, 2019, doi: 10.1039/c8gc03497d.

[16] R. G. D. Andrade, S. R. S. Veloso, and E. M. S. Castanheira, "Shape anisotropic iron oxide-based magnetic nanoparticles: Synthesis and biomedical applications," Int. J. Mol. Sci., vol. 21, no. 7, 2020, doi: 10.3390/ijms21072455.

[17] V. F. Cardoso, A. Francesko, C. Ribeiro, M. Bañobre-López, P. Martins, and S. Lanceros-Mendez, "Advances in Magnetic Nanoparticles for Biomedical Applications," Adv. Healthc. Mater., vol. 7, no. 5, pp. 1–35, 2018, doi: 10.1002/adhm.201700845.

[18] R. Purbia and S. Paria, “Yolk/shell nanoparticles: Classifications, synthesis, properties, and applications,” Nanoscale, vol. 7, no. 47, pp. 19789–19873, 2015, doi: 10.1039/c5nr04729c.

[19] L. A. Kafshgari, M. Ghorbani, and A. Azizi, “Synthesis and characterization of manganese ferrite nanostructure by co-precipitation, sol-gel, and hydrothermal methods,” Part. Sci. Technol., vol. 37, no. 7, pp. 900–906, 2019, doi: 10.1080/02726351.2018.1461154.

[20] M. Srivastava, S. Chaubey, and A. K. Ojha, “Investigation on size dependent structural and magnetic behavior of nickel ferrite nanoparticles prepared by sol-gel and hydrothermal methods,” Mater. Chem. Phys., vol. 118, no. 1, pp. 174–180, 2009, doi: 10.1016/j.matchemphys.2009.07.023.

[21] A. Vioux and P. H. Mutin, “Handbook of Sol-Gel Science and Technology,” Handb. Sol-Gel Sci. Technol., 2017, doi: 10.1007/978-3-319-19454-7.

[22] X. Wang, P. Zhang, J. Gao, X. Chen, and H. Yang, “Facile synthesis and magnetic properties of Fe_3C/C nanoparticles via a sol-gel process,” Dye. Pigment., vol. 112, pp. 305–310, 2015, doi: 10.1016/j.dyepig.2014.07.021.

[23] Z. H. Farooqi, S. R. Khan, R. Begum, and A. Ijaz, “Review on synthesis, properties, characterization, and applications of responsive microgels fabricated with gold nanostructures,” Rev. Chem. Eng., vol. 32, no. 1, pp. 49–69, 2016, doi: 10.1515/revce-2015-0033.

[24] C. Jin, Y. Wang, H. Tang, H. Wei, X. Liu, and J. Wang, “Synthesis, characterization, and catalytic applications of core-shell magnetic carbonaceous nanocomposites,” J. Phys. Chem. C, vol. 118, no. 43, pp. 25110–25117, 2014, doi: 10.1021/jp508853a.

[25] T. Li, M. Cao, J. Liang, X. Xie, and G. Du, “Mechanism of base-catalyzed resorcinol-formaldehyde and phenol-resorcinol-formaldehyde condensation reactions: A theoretical study,” Polymers (Basel)., vol. 9, no. 9, 2017, doi: 10.3390/polym9090426.

[26] J. Oliveira et al., “Carbon-Based Magnetic Nanocarrier for Controlled Drug Release: A Green Synthesis Approach,” C, vol. 5, no. 1, p. 1, 2018, doi: 10.3390/c5010001.

[27] Y. Orooji, S. Mortazavi-Derazkola, S. M. Ghoreishi, M. Amiri, and M. Salavati-Niasari, “Mesopourous Fe_3O_4@SiO_2-hydroxyapatite nanocomposite: Green sonochemical synthesis using strawberry fruit extract as a capping agent, characterization and their application in sulfasalazine delivery and cytotoxicity,” J. Hazard. Mater., vol. 400, no. April, p. 123140, 2020, doi: 10.1016/j.jhazmat.2020.123140.

[28] National Center for Biotechnology Information. PubChem Compound Summary for CID 359, Phloroglucinol. https://pubchem.ncbi.nlm.nih.gov/compound/Phloroglucinol. Accessed Jan. 7, 2022.

[29] National Center for Biotechnology Information. PubChem Compound Summary for CID 5054, Resorcinol. https://pubchem.ncbi.nlm.nih.gov/compound/Resorcinol. Accessed Jan. 7, 2022.

[30] E. Superior, C. Engineering, U. Tecnol, and E. Superior, “Development and functionalization of magnetic nanomaterials for biomedicine applications Thais Sayuri Berberich,” 2020.

[31] M. Bagavathi, A. Ramar, and R. Saraswathi, “Fe3O4–carbon black nanocomposite as a highly efficient counter electrode material for dye-sensitized solar cell,” Ceram. Int., vol. 42, no. 11, pp. 13190–13198, 2016, doi: 10.1016/j.ceramint.2016.05.111.

[32] H. Wang, Q. W. Chen, J. Chen, B. X. Yu, and X. Y. Hu, “Carboxyl and negative charge-functionalized superparamagnetic nanochains with amorphous carbon shell and magnetic core: Synthesis and their application in removal of heavy metal ions,” Nanoscale, vol. 3, no. 11, pp. 4600–4603, 2011, doi: 10.1039/c1nr11012h.

[33] National Center for Biotechnology Information. PubChem Compound Summary for CID 31703, Doxorubicin. https://pubchem.ncbi.nlm.nih.gov/compound/Doxorubicin. Accessed Jan. 7, 2022.

[34] National Center for Biotechnology Information. PubChem Compound Summary for CID 31703, Doxorubicin. https://pubchem.ncbi.nlm.nih.gov/compound/Doxorubicin. Accessed Jan. 7, 2022.